Int. J. Electrochem. Sci., 15 **(2020)** 1264 – 1286, doi: 10.20964/2020.02.02

International Journal of
ELECTROCHEMICAL
SCIENCE
www.electrochemsci.org

Study on Modeling, Experimentation and State of Charge Estimation of Parallel Connected Lithium-ion Batteries

Xin Huang, Xuning Feng, Xuebing Han, Languang Lu, Minggao Ouyang[*]

State Key Laboratory of Automotive Safety and Energy, Tsinghua University, Beijing 100084, P R China
[*]E-mail: ouymg@mail.tsinghua.edu.cn

Received: 18 September 2018 / *Accepted:* 11 November 2018 / *Published:* 31 December 2019

Lithium-ion batteries are always connected in series and parallel to fulfill their functional usage. However, cell variations caused by manufacturing and working conditions can have a great influence on the performance, state of health (SOH), and cell life among the multiple cells in a battery pack. This paper introduces an equivalent circuit model (ECM) for a battery pack composed of several cells connected in parallel. The proposed method simulates current flow distribution among parallel-connected batteries. Meanwhile, a Kalman Filtering algorithm based on the aforementioned ECM is proposed for the state of charge (SOC) estimation of parallel-connected cells. The proposed method has the advantage that very few input variables are needed including only the total current and the total voltage, and the SOC of individual cells can be estimated. The results were validated by experimental data and show good matching accuracy between the model and experimental data. The proposed method provides guidance for additional algorithms that can estimate the individual SOC of cells within a parallel-connected battery pack.

Keywords: lithium-ion battery; parallel-connected; equivalent circuit model; SOC estimation;

1. INTRODUCTION

Lithium-ion batteries play a significant role in the field of energy storage. Large format lithium-ion batteries are becoming a trend of future development, attracting great attention worldwide, owing to reduced pack complexity and thereby improved pack reliability [1-3]. Cell packs are usually connected in parallel by numerous cells to increase cell pack capacity and satisfy the requirement for power. Meanwhile, it is of great importance to investigate transient current distribution in parallel-connected cell packs due to inconsistency in battery management systems. In the short term, the battery SOC [4-6] is affected by imbalanced current distribution, thus causing inconsistency and charge/discharge

variation, while in the long term, the lifetime and reliability of cell packs are undermined seriously and battery degradation is inevitable during battery usage [7-9], with capacity depletion [10-13] and resistance growth [14-17]. Hence, the objective of this paper is to establish a model of parallel-connected cell packs, which can integrate into the existing battery management system and investigate the influence of transient current distribution on the performance of battery packs.

There are few studies on parallel-connected cell packs at present. Prior research has focused on how the performance of parallel-connected cell packs is affected by inconsistency and how the cell packs are constructed in parallel.

Pastor-Fernandez et al. [18] cycled four 3Ah 18650 batteries connected in parallel by charging and discharging 500 times at an ambient temperature of 25℃ to evaluate the degradation over time. The initial capacity difference of 40% converged to 10%, while the initial resistance difference of 45% converged to 30% by the end of cycling. It was also shown that the inconsistency in the current distribution, SOC and temperature between the cells connected in parallel ultimately converged. Gogoana et al. [19] cycled two 2.2Ah LFP batteries connected in parallel with different internal resistances. It was shown that the difference in the lifetime can reach 40%, while the difference in the internal resistance can reach 20% compared to two nearly identical batteries connected in parallel. Yang et al. [20] chose two 2Ah 26650 parallel-connected batteries and established a thermal-electrochemical model using COMSOL software. They found that variations in temperature can add to the inconsistency within the cell packs. The influence of inconsistency on the performance of parallel-connected cells was studied in the above experiments. However, a precise model of parallel-connected cells was not given.

Spurret et al. [21] established a model of parallel-connected cells. In the model, each single cell comprised the open circuit voltage source, internal resistance and leakage current. Simulation results showed that the internal resistance increased rapidly due to battery aging. Fouchard et al. [22] studied the imbalance current inside cell packs connected in parallel. The results advised avoiding the use of parallel-connected cells owing to safety issues caused by the failure of a single cell. Cole et al. [23] investigated the current distribution inside parallel-connected lead acid batteries. The experimental results showed that the current was divided in proportion to the capacity of each cell. Zhang et al. [24] introduced a model of series-and-parallel-connected cells and investigated the current distribution under different working conditions. Wu et al. [25] introduced a numerical model that simulated batteries connected in parallel with diverse capacities and analyzed the current distribution under different charge/discharge current rates. Shi et al. [26] cycled four cells connected in parallel with different capacities and resistances under different charge/discharge current rates. It was identified that an imbalanced current distribution within cell packs was the main cause of the degradation of cell packs. Weng et al. [27] analyzed the IC curve of parallel-connected cells, and the results showed that there existed a certain relationship between the peak value of the IC curve and the aged battery capacity. An et al. [28] introduced an equivalent circuit model of parallel-connected cells and proposed an index of variation to evaluate cell packs. Dubarry et al. [29] proposed a method to analyze the current distribution of cell packs connected in different series-parallel configurations and verified the experimental results. Offer et al. [30] simulated a 12P7S cell pack using Simulink Sim Power Systems software and investigated the current distribution under different working conditions. Miyatake et al. [31] connected different types of 18650 batteries in series and parallel, introduced a model in which the Rint model was

used for each single cell, and investigated the influence of different model parameters on the current distribution.

However, until now, no publication has described in detail a precise equivalent circuit model applied for the analysis of dynamic current distribution inside parallel-connected cells, and the SOC estimation of each single cell inside parallel-connected cells has not been thoroughly researched [36].

Based on this, an equivalent circuit model (ECM) of cell packs composing several cells connected in parallel is introduced in this paper, which is coupled with equivalent circuit models of several single cells. The parameters within the equivalent circuit model of a single cell are identified by methods such as the genetic algorithm and the recursive least square algorithm. Meanwhile, the battery open circuit voltage V_{oc} and polarization voltage drop V_P are chosen as state variables by applying state space theory and Kirchhoff's current and voltage law are utilized to establish the ECM of cell packs. Furthermore, a Kalman filtering algorithm based on the aforementioned ECM is proposed for the SOC estimation of each single cell inside the cell pack connected in parallel [32]. The total current and total voltage of the parallel-connected cell pack are used as input variables in the ECM, which is linearized by the method of extended Kalman filtering, and the equivalent circuit model of a single cell is discretized. The advantage of this method is that there are very few input variables, including only the total current and total voltage, and the SOC estimation of each single cell inside the cell pack is performed in situ with good accuracy.

In Section 2, a brief summary of the experiment and apparatus is introduced. In Section 3, the modeling approach of the ECM of parallel-connected cells is introduced. Based on this, Section 4 validates the ECM by experiment and applies the model for SOC estimation. The conclusions of this study are presented in Section 5.

2. EXPERIMENTAL PROCEDURE

Three NCM batteries with 37 Ah nominal capacity were chosen and connected in parallel. The specifications of the batteries are listed in Table 1. To establish the ECM of a single cell, cell characterization of each cell was performed, and the details are listed in Sec. 2.1: Cell Characterization. Meanwhile, to establish the ECM of parallel-connected cells, the charge/discharge test was performed on the batteries, and the details are listed in Sec. 2.2: Parallel-Connected Cells Testing.

Table 1. Specifications of NCM Cells

No.	Items	Symbol	Specifications
1	battery type	-	$Li(Ni_xCO_yMn_z)O_2$
2	nominal capacity	Q_{nom}	37Ah
3	end-of-charge voltage	V_{EOC}	4.2V
4	end-of-discharge voltage	V_{EOD}	2.8V
5	maximum current	I_{max}	6C (continuous) 8C (10s, @50%SOC)

2.1 Cell Characterization

Cell characterization consists of three tests: battery capacity measurement, open circuit voltage measurement, and impedance measurement.

Battery capacity measurement: This test was used to obtain the battery capacity under different current rates. To measure capacity, each cell was set aside at 25℃ ambient temperature for 3 h until the equilibrium state was reached; then, each cell was subjected to constant current constant voltage charging (1/20C, 1/3C, 1C) until the battery voltage reached V_{EOC} according to the manufacturer's specifications; Then, each cell was set aside at 25℃ ambient temperature for 1 h until the equilibrium state was reached; Then, each cell was subjected to constant current constant voltage discharging (1/20C, 1/3C, 1C) until the battery voltage reached V_{EOD} according to the manufacturer's specifications. The charge accumulated up from V_{EOC} to V_{EOD} is assumed as the battery capacity.

Open circuit voltage measurement: The battery V_{oc} ~ SOC curve was obtained by discharging each cell at 1/20C from 100% SOC and normalizing the results against the 1/3C capacity. Because the 1/20C current is sufficiently low, the effect of impedance is negligible, and the terminal voltage is approximately equal to the open circuit voltage.

Impedance measurement: Each cell was analyzed using the HPPC test, as shown in Figure 1, and the data obtained were used to fit the ECM of a single cell. The test procedure was as follows: each cell was discharged at 1/3C from 100% SOC until the battery voltage reached V_{EOD}; every increment of 5% SOC, each cell was subjected to one pulse current, which was composed of a 30 s discharge current at 1C, a 40 s rest, a 30 s charge current at 1C and a 30 min rest; and then, each cell was set aside at 25℃ ambient temperature for 3 h until the equilibrium state was reached.

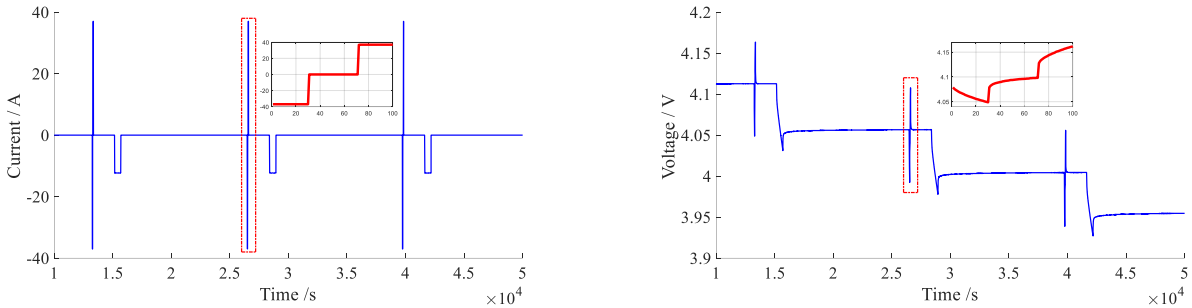

(a) (b)

Figure 1. The HPPC test. (a)current file, (b) voltage file

2.2 Parallel-Connected Cells Testing

Three NCM cells were connected in parallel in the experiment, and they were linked together with copper conductors, each of which was surrounded by a LEM Hall effect current sensor LFP100 to measure the current running through each cell. The range of the current sensor is 0~±150 A, and the tracking accuracy exceeds 200 A/μs, and the measuring accuracy equals to 0.45% at 25℃ ambient temperature. The data obtained were logged into a 64-channel data logger. The whole apparatus was

placed inside a Bell temperature chamber, which operates under the control of -40℃~150℃. A Neware 8-channel test bench, which operates under the range of 0~5 V and 0~100 A, was used to control the applied current into the parallel-connected cells. The specifications of the test equipment are listed in Table 2.

Table 2. Test Equipment

No.	Items	Manufacturer	Specifications
1	Test bench	Neware	0~5V,0~100A
2	Thermal chamber	Bell	-40~150℃
3	Current sensor	LEM	Hall type,0~±150A >200A/μs,±0.45%
4	Data logger	Neware	64 channels

To meet the requirements of establish the ECM, three typical operating conditions were chosen for the parallel-connected cells, as shown in Table 3, including the constant current charge/discharge process and the dynamic stress test (DST). Testing standards consisting of current profiles are shown in Figure 2.

Table 3. Typical Operating Conditions for Batteries Connected in Parallel

No.	Operating Condition
1	Steady discharge process from 100% SOC to cut-off voltage under 1C rate
2	Steady charge process from 0% SOC to cut-off voltage under 1C rate
3	Dynamic stress test under maximum current 2C rate

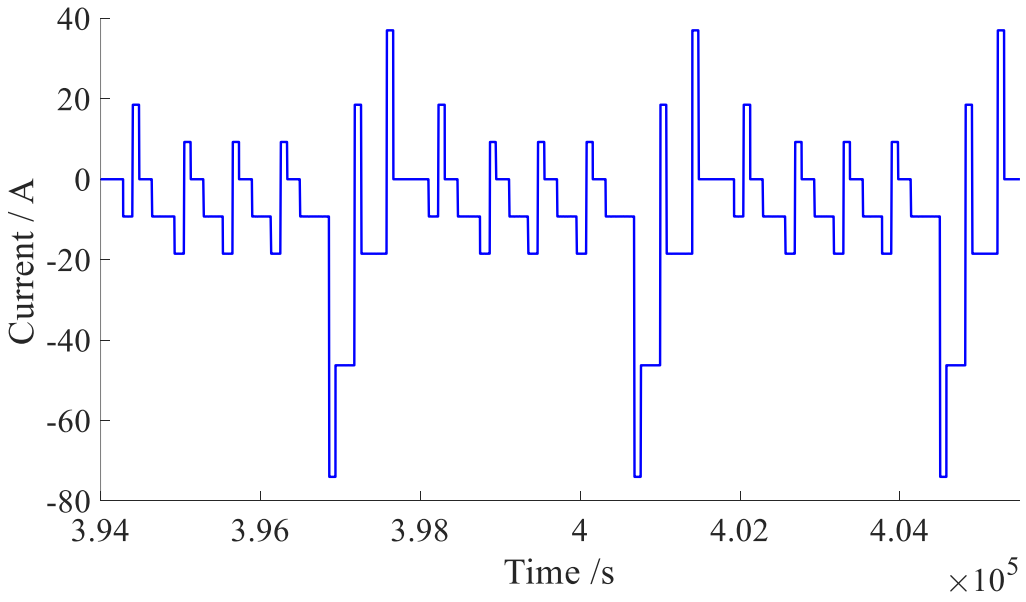

Figure 2. parallel-connected cells DST test current profiles

3. THEORETICAL PROCEDURE

3.1 Equivalent circuit model for a single cell

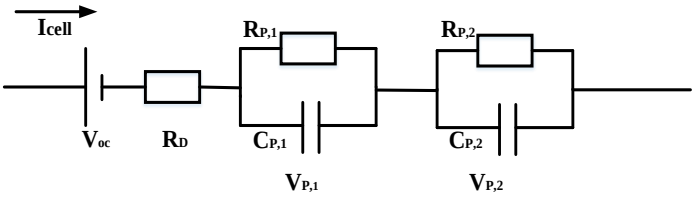

Figure 3. ECM with two RC pairs for single cell

Figure 3 describes the ECM with two resistor-capacitor (RC) pairs for a single cell, and the specific formula is shown in Equation (1), which indicates that, the battery terminal voltage equals the sum of the open circuit voltage V_{oc}, the direct current voltage drop over the internal resistance $R_D I_{cell}$, and the polarization voltage drop over the RC pairs V_P at a given current I_{cell}. In Equation (1), considering the accuracy and complexity of the ECM, two RC pairs are chosen for this system. Equation (2) describes the polarization voltage drop over the RC pairs V_P, while Equation (3) describes the battery SOC, for which R_P and C_P represent the polarization resistance and capacitance over the RC pairs, respectively, and Q_{cell} represents the battery standard capacity. The open circuit voltage is determined by the battery SOC, which can be acquired by experiment, as shown in Equation (4).

$$V_t = V_{oc} + R_D I_{cell} + V_{P,1} + V_{P,2} \quad (1)$$

$$\overset{g}{V}_{P,i} = -\frac{V_{P,i}}{R_{P,i} C_{P,i}} + \frac{I_{cell}}{C_{P,i}} \quad (i = 1, 2) \quad (2)$$

$$\overset{g}{SOC} = \frac{I_{cell}}{3600 Q_{cell}} \quad (3)$$

$$V_{oc} = f(SOC) \quad (4)$$

The ECM of a single cell consists of four equations, as mentioned above, which can be transformed into a state space matrix. Generally, *SOC* and V_P are chosen as the state variables. To connect cells in parallel in mathematical form, V_{oc}, V_{P1}, and V_{P2} are chosen as state variables in this paper according to Kirchhoff's voltage law. The state space matrix of the ECM of a single cell is described as follows.

Equation (5) presents the chosen state variable *x*. Equation (6) defines the effective charge *M*, which represents the charge needed for a single cell at a given open circuit voltage variation. The nonlinear part is transferred from the output matrix *C* to the input matrix *B* by the effective charge *M*. This nonlinear part represents the gradient of the $V_{oc} \sim SOC$ curve of a single cell. In addition, according to Equation (3), the differential of the open circuit voltage V_{oc} can be derived in Equation (7).

The current running through a single cell I_{cell} is chosen as the input variable *u*, and the terminal voltage V_t is chosen as the output variable *y*, as described in Equation (7) and Equation (8). Equation (11) presents the state space matrix, and Equations (12) ~ (15) present the state matrix *A*, input matrix *B*, output matrix *C* and feedforward matrix *D*, respectively.

$$x=\begin{bmatrix} V_{oc} \\ V_{p1} \\ V_{p2} \end{bmatrix} \tag{5}$$

$$M=3600Q_{cell}\frac{dSOC}{dV_{oc}} \tag{6}$$

$$\overset{\text{g}}{V}_{oc}=\frac{dV_{oc}}{dt}=\frac{dV_{oc}}{dSOC}\frac{dSOC}{dt}=\frac{dV_{oc}}{dSOC}\frac{I_{cell}}{3600Q_{cell}}=\frac{I_{cell}}{3600Q_{cell}\dfrac{dSOC}{dV_{oc}}}=\frac{I_{cell}}{M} \tag{7}$$

$$\begin{cases} \overset{\text{g}}{x}=Ax+Bu \\ y=Cx+Du \end{cases} \tag{8}$$

$$u=I_{cell} \tag{9}$$

$$y=V_t \tag{10}$$

$$\begin{bmatrix} \overset{\text{g}}{V}_{oc} \\ \overset{\text{g}}{V}_{P1} \\ \overset{\text{g}}{V}_{P2} \end{bmatrix}=\begin{bmatrix} 0 & 0 & 0 \\ 0 & -\dfrac{1}{R_{P1}C_{P1}} & 0 \\ 0 & 0 & -\dfrac{1}{R_{P2}C_{P2}} \end{bmatrix}\begin{bmatrix} V_{oc} \\ V_{P1} \\ V_{P2} \end{bmatrix}+\begin{bmatrix} \dfrac{1}{M} \\ \dfrac{1}{C_{P1}} \\ \dfrac{1}{C_{P2}} \end{bmatrix}\begin{bmatrix} I_{cell} \end{bmatrix} \tag{11}$$

$$\begin{bmatrix} V_t \end{bmatrix}=\begin{bmatrix} 1 & 1 & 1 \end{bmatrix}\begin{bmatrix} V_{oc} \\ V_{p1} \\ V_{p2} \end{bmatrix}+\begin{bmatrix} R_D \end{bmatrix}\begin{bmatrix} I_{cell} \end{bmatrix}$$

$$A=\begin{bmatrix} 0 & 0 & 0 \\ 0 & -\dfrac{1}{R_{P1}C_{P1}} & 0 \\ 0 & 0 & -\dfrac{1}{R_{P2}C_{P2}} \end{bmatrix} \tag{12}$$

$$B=\begin{bmatrix} \dfrac{1}{M} \\ \dfrac{1}{C_{P1}} \\ \dfrac{1}{C_{P2}} \end{bmatrix} \tag{13}$$

$$C=[1 \quad 1 \quad 1] \tag{14}$$

$$D=\begin{bmatrix} R_D \end{bmatrix} \tag{15}$$

3.2 Equivalent circuit model for N batteries connected in parallel

Single cells, as shown in Figure 4(b), can be extended into the ECM for N cells connected in parallel as shown in Figure 4(a). $I_{cell,k}$ represents the current running through the *k*-th cell, while I_k represents the current running through the *k*-th current loop. Meanwhile, $R_{w,k}$ represents the wire resistance of the *k*-th current loop, while $R_{c,k}$ represents the contact resistance of the *k*-th current loop.

Furthermore, the *k*-th current loop is shown in Figure 5, which contains the *k-1*-th and *k*-th cells, and the *k-1*-th and *k*-th junctions. In each current loop, two constraints must be satisfied in the ECM, and they are the Kirchhoff's current and voltage laws.

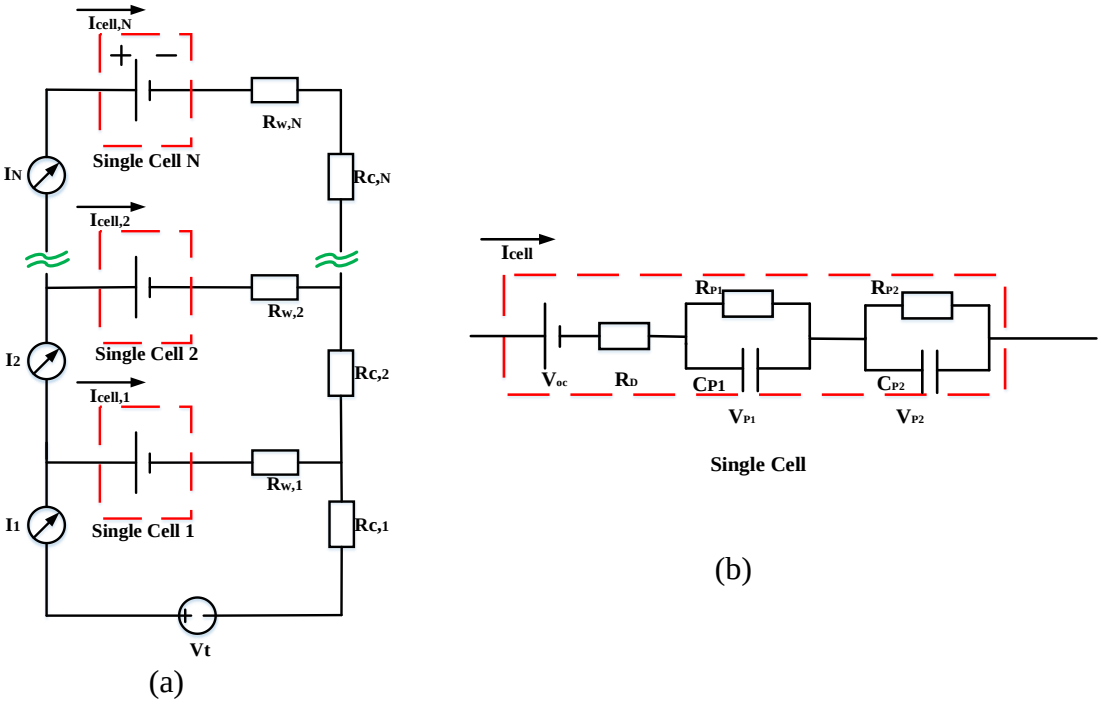

Figure 4. ECM for N batteries connected in parallel, (a) N batteries connected in parallel, (b) single cell

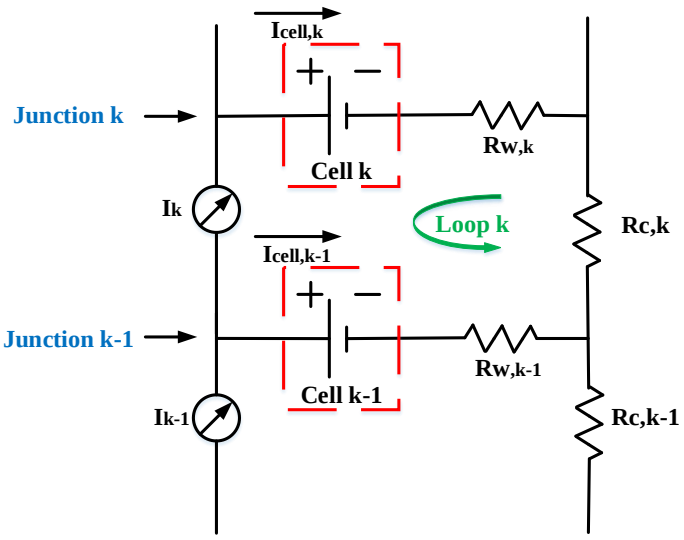

Figure 5. the *k* th current loop in the N batteries connected in parallel

According to Kirchhoff's current law, in the *k*-th junction of the *k*-th current loop in the parallel-connected cells, the input current equals to output current at any time. As shown in Equation (16), the output current I_k equals the sum of the input currents I_{k-1} and $I_{cell,k}$ for *k*<N, while the output current I_k equals to the input current $I_{cell,k}$ for k=N. Hence, Equation (17) can be derived, thus defining matrix *H* in Equation (18).

$$\begin{cases} 0 = I_k - I_{k+1} - I_{cell,k} & k < N \\ 0 = I_k - I_{cell,k} & k = N \end{cases} \tag{16}$$

$$\begin{bmatrix} I_{cell,1} \\ I_{cell,2} \\ \cdots \\ I_{cell,N} \end{bmatrix} = \begin{bmatrix} 1 & -1 & 0 & 0 \\ 0 & 1 & -1 & 0 \\ 0 & .... & 1 & -1 \\ 0 & ... & 0 & 1 \end{bmatrix} \begin{bmatrix} I_1 \\ I_2 \\ ... \\ I_N \end{bmatrix} \tag{17}$$

$$H = \begin{bmatrix} 1 & -1 & 0 & 0 \\ 0 & 1 & -1 & 0 \\ 0 & .... & 1 & -1 \\ 0 & ... & 0 & 1 \end{bmatrix} \tag{18}$$

According to Kirchhoff's voltage law, the algebraic sum of the voltage drop over every component in the *k* th current loop is equal to zero. Hence, Equation (19) can be derived.

$$\begin{cases} 0 = V_{oc,k} - V_{oc,k-1} + V_{P1,k} - V_{P1,k-1} + V_{P2,k} - V_{P2,k-1} + (R_{D,k} + R_{w,k})(I_k - I_{k+1}) - (R_{D,k-1} + R_{w,k-1})(I_{k-1} - I_k) + R_{c,k} I_k & k < N \\ 0 = V_{oc,k} - V_{oc,k-1} + V_{P1,k} - V_{P1,k-1} + V_{P2,k} - V_{P2,k-1} + (R_{D,k} + R_{w,k}) I_k - (R_{D,k-1} + R_{w,k-1})(I_{k-1} - I_k) + R_{c,k} I_k & k = N \end{cases} \tag{19}$$

Furthermore, as shown in Equation (20), the state space matrix of N cells connected in parallel can be derived from Equation (11). Thus, $A_1 \sim A_N$, $B_1 \sim B_N$, $C_1 \sim C_N$, and $D_1 \sim D_N$ represent the state matrix, input matrix, output matrix and feedforward matrix respectively. Meanwhile, the state variable *X* of the ECM of parallel-connected cells is defined in Equation (21) by extension of the state variable *x* of single cell in Equation (5). Meanwhile, the state matrix A_X, input matrix B_X, output matrix C_X and feedforward matrix D_X are defined in Equations (22) ~ (25), respectively.

$$\begin{bmatrix} \overset{g}{x}_1 \\ \overset{g}{x}_2 \\ \cdots \\ \overset{g}{x}_N \end{bmatrix} = \begin{bmatrix} A_1 & & & \\ & A_2 & & \\ & & \cdots & \\ & & & A_N \end{bmatrix} \begin{bmatrix} x_1 \\ x_2 \\ \cdots \\ x_N \end{bmatrix} + \begin{bmatrix} B_1 & & & \\ & B_2 & & \\ & & \cdots & \\ & & & B_N \end{bmatrix} \begin{bmatrix} I_{cell,1} \\ I_{cell,2} \\ \cdots \\ I_{cell,N} \end{bmatrix} \tag{20}$$

$$\begin{bmatrix} V_t \end{bmatrix} = \begin{bmatrix} C_1 & 0 & 0 & 0 \end{bmatrix} \begin{bmatrix} x_1 \\ x_2 \\ \cdots \\ x_N \end{bmatrix} + \begin{bmatrix} (D_1 + R_{w,1} + R_{c,1}) & R_{c,1} & \cdots & R_{c,1} \end{bmatrix} \begin{bmatrix} I_{cell,1} \\ I_{cell,2} \\ \cdots \\ I_{cell,N} \end{bmatrix}$$

$$X = \begin{bmatrix} x_1 \\ x_2 \\ \cdots \\ x_N \end{bmatrix} \quad (21)$$

$$A_X = \begin{bmatrix} A_1 & & & \\ & A_2 & & \\ & & \cdots & \\ & & & A_N \end{bmatrix} \quad (22)$$

$$B_X = \begin{bmatrix} B_1 & & & \\ & B_2 & & \\ & & \cdots & \\ & & & B_N \end{bmatrix} \quad (23)$$

$$C_X = \begin{bmatrix} C_1 & 0 & 0 & 0 \end{bmatrix} \quad (24)$$

$$D_X = \begin{bmatrix} (D_1 + R_{w,1} + R_{c,1}) & R_{c,1} & \cdots & R_{c,1} \end{bmatrix} \quad (25)$$

Equation (19) derived from Kirchhoff's voltage law can be transformed into a matrix expression, as shown in Equation (26), among which matrices *G*, *E*, and *F* are defined in Equation (27), Equation (28) and Equation (29), respectively. Equation (26) describes the relationship between the loop current and state variable *X*.

$$G \begin{bmatrix} I_1 \\ I_2 \\ \cdots \\ I_N \end{bmatrix} = EX + FI_1 \quad (26)$$

$$G = \begin{bmatrix} 1 & 0 & 0 & 0 \\ 0 & -(R_{D,1} + R_{w,1} + R_{D,2} + R_{w,2} + R_{c,2}) & R_{D,2} + R_{w,2} & 0 \\ 0 & R_{D,2} + R_{w,2} & \cdots & R_{D,N-1} + R_{w,N-1} \\ 0 & 0 & R_{D,N-1} + R_{w,N-1} & -(R_{D,N-1} + R_{w,N-1} + R_{D,N} + R_{w,N} + R_{c,N}) \end{bmatrix} \quad (27)$$

$$E = \begin{bmatrix} 0 & 0 & \cdots & & & & 0 \\ -1 & -1 & 1 & 1 & 0 & \cdots & 0 \\ 0 & -1 & -1 & 1 & 1 & \cdots & 0 \\ 0 & 0 & \cdots & & & & 0 \\ 0 & 0 & \cdots & & & & 0 \\ 0 & 0 & \cdots & & & & 0 \\ 0 & \cdots & 0 & -1 & -1 & 1 & 1 \end{bmatrix} \quad (28)$$

$$F = \begin{bmatrix} 1 \\ -(R_{D,1} + R_{c,1}) \\ 0 \\ \cdots \\ 0 \end{bmatrix} \quad (29)$$

Furthermore, Equation (30) is derived by the combination of Equation (17) and Equation (26), and it represents the relationship between the current distribution inside parallel-connected cells and state variable X.

$$\begin{bmatrix} i_{cell,1} \\ i_{cell,2} \\ \cdots \\ i_{cell,N} \end{bmatrix} = HG^{-1}(EX + FI_1) \quad (30)$$

Based on the state space theory, the total current running through parallel-connected cells I_1 is chosen as input variable U, and terminal voltage V_t is chosen as output variable Y, as described in Equations (31) ~ (33). Thus, the state space matrix of parallel-connected cells, as shown in Equation (34), is derived by the combination of Equation (20) and Equation (30). Meanwhile, A', B', C', and D' represent the state matrix, input matrix, output matrix and feedforward matrix of the ECM of parallel-connected cells, respectively.

$$\begin{cases} \dot{X} = A'X + B'U \\ Y = C'X + D'U \end{cases} \quad (31)$$

$$U = I_1 \quad (32)$$

$$Y = V_t \quad (33)$$

$$\begin{aligned} A' &= A_X + B_X HG^{-1}E \\ B' &= B_X HG^{-1}F \\ C' &= C_X + D_X HG^{-1}E \\ D' &= D_X HG^{-1}F \end{aligned} \quad (34)$$

4. RESULTS AND DISCUSSION

4.1 Model Validation

A modeling method to simulate N cells connected in parallel is proposed. Three 37 Ah NCM batteries were chosen in this paper. First, the parameters of the ECM of each cell were identified by the genetic algorithm, and the accuracy of each model was validated by experiment, as shown in Sec 4.1; Then, the charge/discharge procedure of parallel-connected cells was conducted under different operating conditions, and the accuracy of the ECM of parallel-connected cells was validated, as shown in Sec 4.2.

4.1.1 Experimental validation of the ECM for cells

The capacities of each NCM cell under different current rates are listed in Table 4. The capacity of Cell No. 2 is approximately equal to that of Cell No. 3, while the capacity of Cell No. 1 is larger than that of the other two cells. The OCV vs. SOC curves of these three cells are presented in Figure 6(a), in

which the three curves are basically consistent. Figure 6(b) displays the gradient of the OCV vs. SOC curve of Cell No. 1, in which the gradient value is positive in the whole SOC region. This result means that the OCV monotonically increases with increasing SOC. The gradient value of OCV vs. SOC curve is applied in Equation (11).

Table 4. Capacity under different charge/discharge rate for each cell (Ah)

Cell	1/20C		1/3C		1C	
	Charge	Discharge	Charge	Discharge	Charge	Discharge
1	42.9	42.11	40.20	40.125	39.08	39.03
2	41.64	41.43	39.52	39.51	38.38	38.35
3	41.67	41.4	39.66	39.575	38.65	38.46

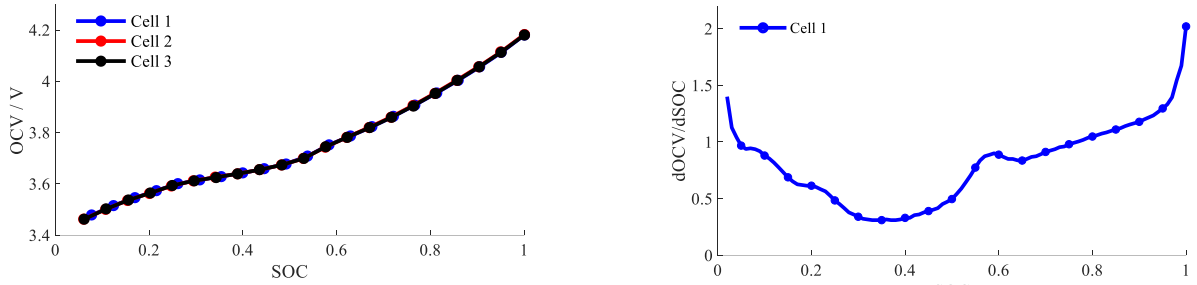

Figure 6. OCV vs SOC curve of each cell, (a) OCV vs SOC curve, (b) gradient of OCV vs SOC curve

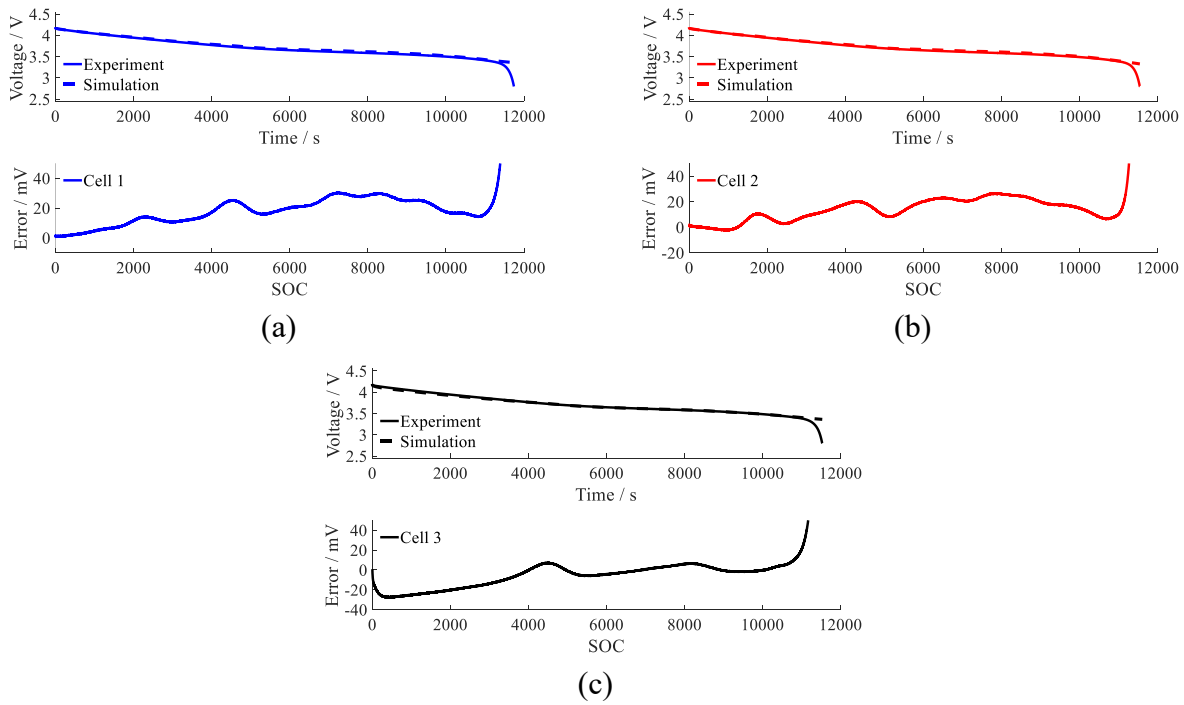

Figure 7. Experimental Validation of the accuracy of ECM for single cell, solid line = experiment, dashed line = model, (a) accuracy for Cell 1, (b) accuracy for Cell 2, (c) accuracy for Cell 3

The open circuit voltage of each cell was obtained by the HPPC experiment, while five parameters of the ECM of each cell, i.e., R_D, R_{P1}, R_{P2}, C_{P1}, *and* C_{P2}, were derived by the genetic algorithm method. These parameters are strongly related to the battery SOC. Figure 7 shows the model accuracy of the ECM of the three cells investigated in this paper. The model error was less than ±30 mV in the high SOC region.

4.1.2 Experimental validation of the ECM for batteries connected in parallel

Three typical operating conditions were chosen for validation of the ECM for batteries connected in parallel by experiment, including the steady charge/discharge process and the dynamic stress test, as shown in Table 3. The results are demonstrated in Figure 8 ~ Figure 10, which show that the ECM accuracy is relatively high not only in the steady test but also in the dynamic test.

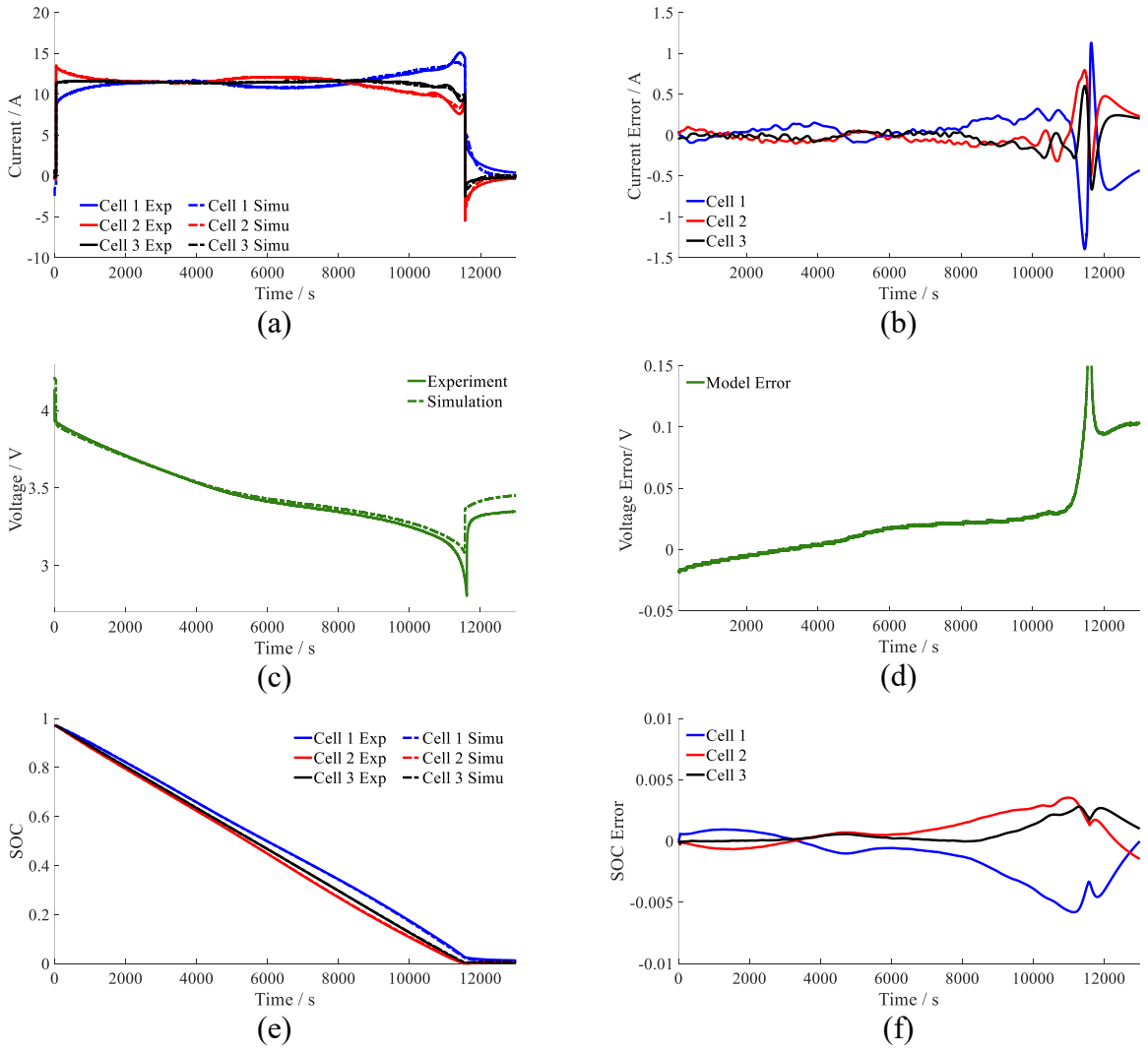

Figure 8. Experimental Validation of ECM under operating condition No.1 for batteries connected in parallel, solid line = experiment, dashed line = model, (a) current distribution for each cell, (b) current distribution error for each cell, (c) terminal voltage for experiment and model, (d) terminal voltage error, (e) SOC for each cell, (f) SOC error for each cell

The ECM validation results of the steady discharge process are presented in Figure 8. The solid line represents the experimental results and the dashed line represents model results. The current distribution and current error obtained by experiment and the model are shown in Figure 8(a) ~ (b). This phenomenon of imbalanced current distribution is also observed in other papers [19,26,33-34].

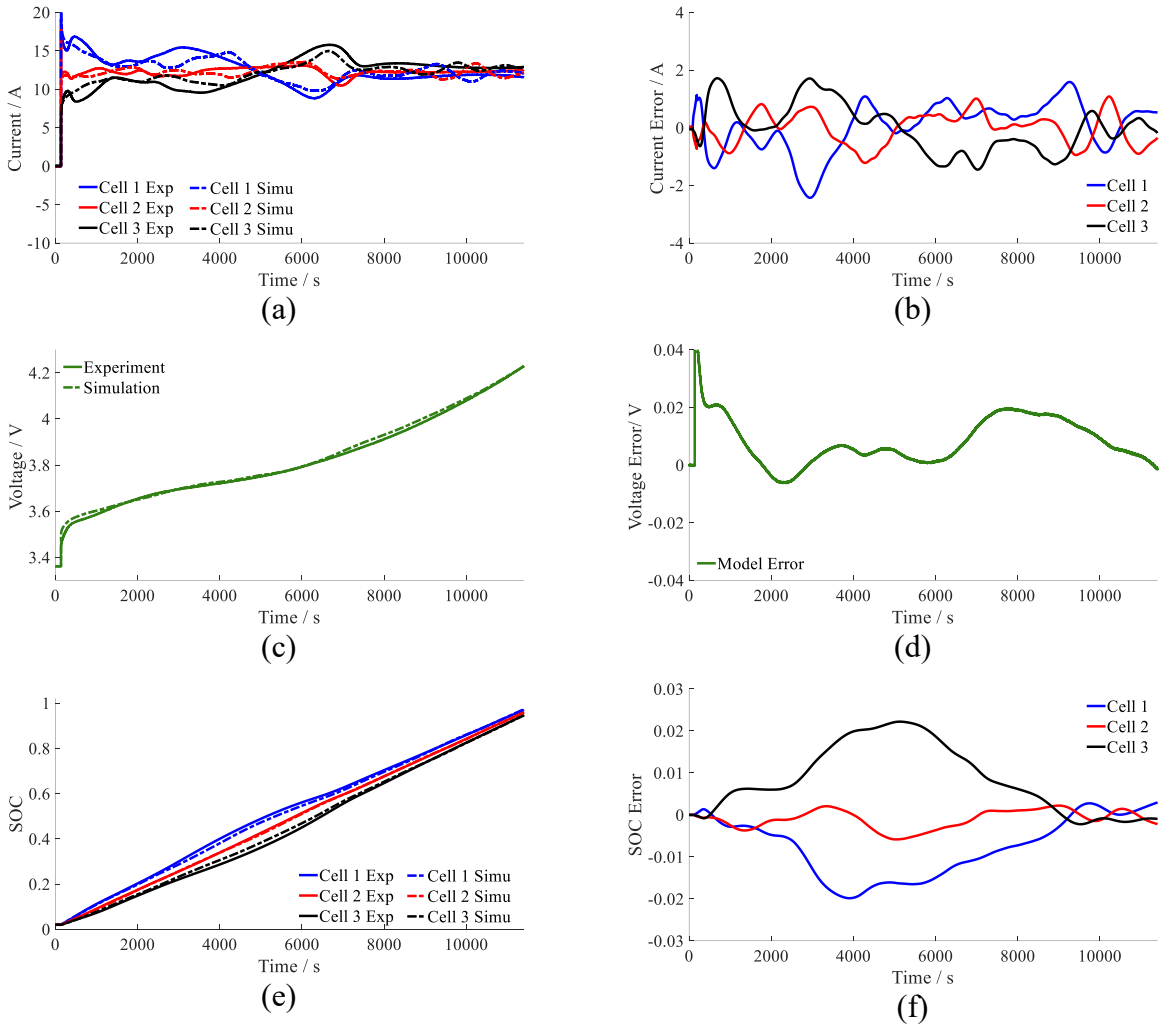

Figure 9. Experimental Validation of ECM under operating condition No.2 for batteries connected in parallel, solid line = experiment, dashed line = model, (a) current distribution for each cell, (b) current distribution error for each cell, (c) terminal voltage for experiment and model, (d) terminal voltage error, (e) SOC for each cell, (f) SOC error for each cell

The current error was less than 0.5 A in the medium and high SOC regions, while the current error was relatively high in the low SOC region, which was caused by the poor accuracy of the two-pair RC model used in the ECM. A similar phenomenon appeared in the terminal voltage presented in Figure 8(c) ~ (d). The terminal voltage error was less than 50mV in the medium and high SOC regions. The SOC results and error are presented in Figure 8(e) ~ (f). The SOC simulation was quite precise with only 0.5% SOC error. Hence, it can be concluded that the model accuracy of the ECM of cells connected in parallel was relatively high in the steady discharge process.

The ECM validation results of the steady charge process are presented in Figure 9. The solid line represents experimental results and the dashed line represents model results. The current distribution and current error obtained by experiment and the model are shown in Figure 9(a) ~ (b).

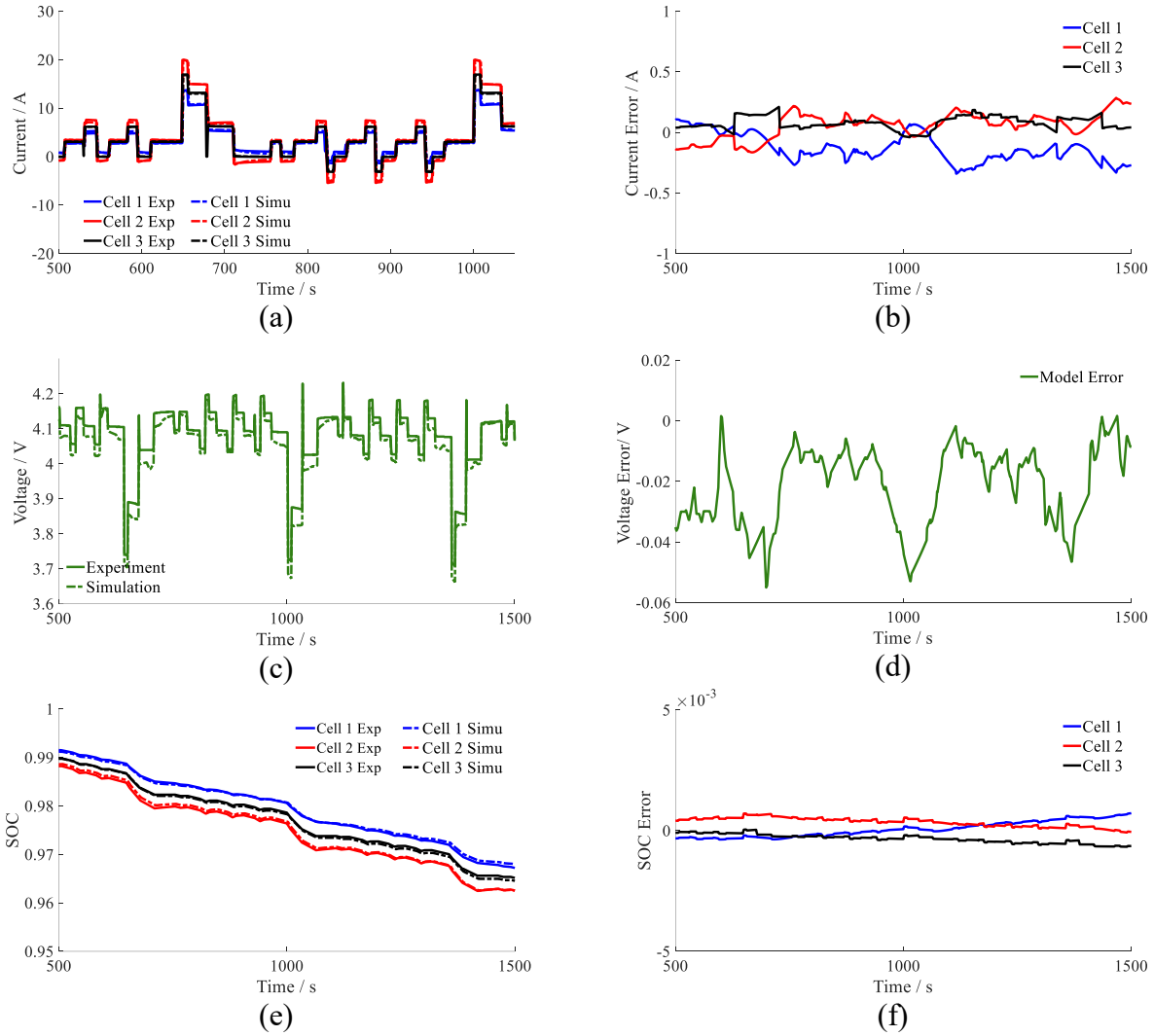

Figure 10. Experimental Validation of ECM under operating condition No.3 for batteries connected in parallel, solid line = experiment, dashed line = model, (a) current distribution for each cell, (b) current distribution error for each cell, (c) terminal voltage for experiment and model, (d) terminal voltage error, (e) SOC for each cell, (f) SOC error for each cell

The current error was less than 2A in the medium and high SOC regions, while the current error was relatively high in the low SOC regions. The terminal voltage results and error are presented in Figure 9(c) ~ (d). The terminal voltage error was less than 50mV in the medium and high SOC regions. Figure 9(e) ~ (f) describes the SOC results and error. The SOC simulation was quite precise with only 2% SOC error. Hence, it can be concluded that the model accuracy of the ECM of cells connected in parallel was relatively high in the steady charge process.

The ECM validation results of the dynamic stress test are presented in Figure 10. The solid line represents experimental results and the dashed line represents the model results. The current distribution and current error obtained by experiment and the model are shown in Figure 10(a) ~ (b). The current error was less than 0.5 A in the medium and high SOC regions, while the current error was relatively high in the low SOC region. A similar phenomenon appeared in the terminal voltage presented in Figure 10(c) ~ (d). The terminal voltage error was less than 50 mV in the medium and high SOC regions. The SOC results and error are presented in Figure 10(e) ~ (f). The SOC simulation was quite precise with only 0.5% SOC error. Hence, it can be concluded that the model accuracy of the ECM of cells connected in parallel was relatively high in the dynamic stress test.

4.2 Modelling Analysis

4.2.1 Current Distribution

The total battery current and total battery voltage are input variables of the ECM for cells connected in parallel. The current distribution inside parallel-connected cells can be derived by simulation. Given the aforementioned model validation results, it can be determined that the ECM established by the above method has good adaptability to both the steady charge/discharge process and the dynamic stress test.

The principle of current distribution inside parallel-connected cells is deduced in the following equations according to the relationships among the current distribution, battery capacity and internal resistance with the ECM reducing to the Rint model.

For the whole battery module and the single cell, the following can be obtained:

$$R_{cell,1}i_{cell,1}+V_{oc,1}=R_{cell,2}i_{cell,2}+V_{oc,2}=R_{cell,3}i_{cell,3}+V_{oc,3} \quad (35)$$

For the single cell, it can be obtained that,

$$V_t=V_{oc}+R_D i_{cell} \quad (36)$$

$$\dot{SOC}=\frac{i_{cell}}{3600Q_{cell}} \quad (37)$$

$$V_{oc}=f(SOC) \quad (38)$$

- Assuming consistent internal resistance and initial SOC and different battery capacity inside the battery module in the discharge process

In the initial discharge process, due to cells connected in parallel, the initial SOC and OCV are consistent, thus producing equal initial current inside the parallel-connected cells. When the discharge process begins, due to different battery capacities, the SOC of different cells differ, thus causing different OCVs in the different cells. Therefore, the current distribution inside cells connected in parallel differs. The specific derivation procedure is presented in Equation (39) ~ Equation (42).

$$Q_1>Q_2>Q_3 \quad (39)$$

$$\Delta SOC_1<\Delta SOC_2<\Delta SOC_3 \quad (40)$$

$$SOC_1>SOC_2>SOC_3 \quad (41)$$

$$i_1>i_2>i_3 \quad (42)$$

△SOC of different cells converges after long-term stabilization. The current distribution inside the battery module is shown in Equation (43) ~ Equation (44).

$$\Delta SOC_1 = \Delta SOC_2 = \Delta SOC_3 \quad (43)$$

$$i_1 / Q_1 = i_2 / Q_2 = i_3 / Q_3 \quad (44)$$

The simulation results of the current distribution inside cells connected in parallel under the aforementioned assumption are presented in Figure 11(a). Figure 11(b) describes the total current applied. The simulation results and theoretical derivation results were consistent.

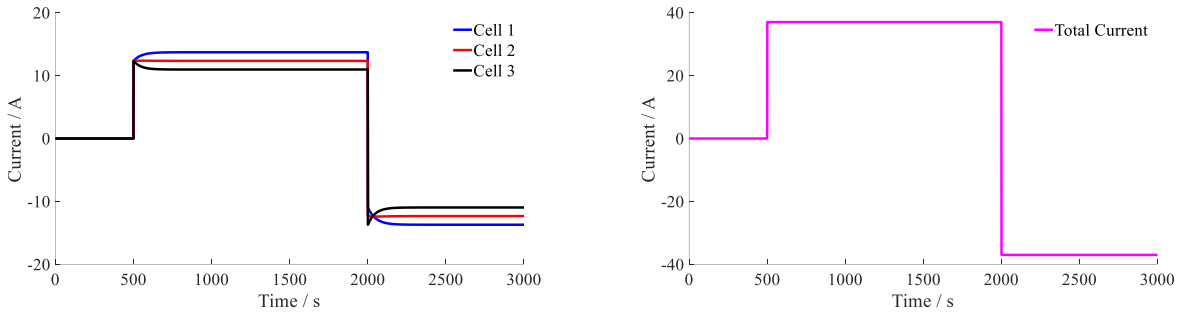

(a) (b)

Figure 11. Current distribution under the hypothesis of different capacity and unanimous internal resistance (a) current distribution of different cells (b) working condition

- Assuming consistent battery capacity and initial SOC and different internal resistance inside the battery module in the discharge process

In the initial discharge process, due to cells connected in parallel, the initial SOC and OCV are consistent. Therefore, the initial current is inversely proportional to the battery internal resistance, as presented in Equation (45) ~ Equation (46).

$$R_1 i_1 = R_2 i_2 = R_3 i_3 \quad (45)$$

$$i_1 < i_2 < i_3 \quad (46)$$

Given that the △SOC of different cells converges after long-term stabilization, the current distribution inside the battery module also converges because of the consistent battery capacity, as shown in Equation (47) ~ Equation (49).

$$\Delta SOC_1 = \Delta SOC_2 = \Delta SOC_3 \quad (47)$$

$$i_1 / Q_1 = i_2 / Q_2 = i_3 / Q_3 \quad (48)$$

$$i_1 = i_2 = i_3 \quad (49)$$

Figure 12(a) demonstrates the simulation results of the current distribution inside cells connected in parallel under the aforementioned assumption. The total current applied is presented in Figure 12(b). The simulation results and theoretical derivation results were consistent.

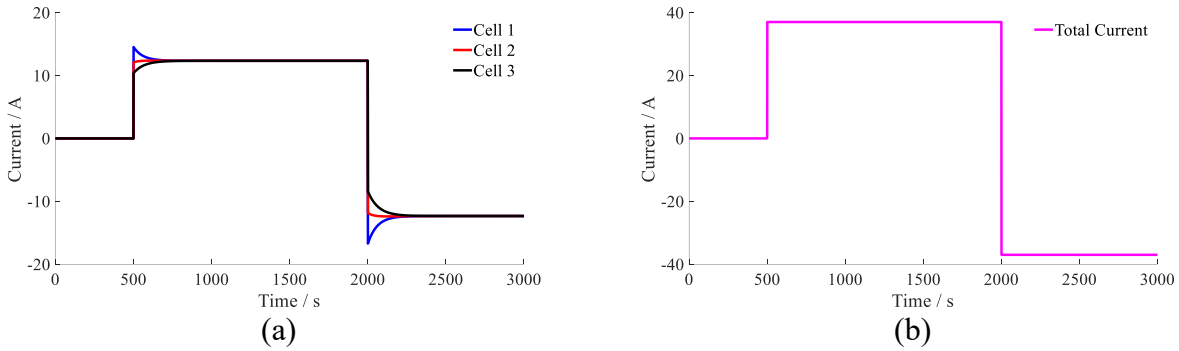

Figure 12. Current distribution under the hypothesis of different internal resistance and unanimous capacity (a) current distribution of different cells (b) working condition

4.2.2 State Estimation using Kalman Filtering

A Kalman Filtering algorithm [35] based on the aforementioned ECM is proposed for the SOC estimation of each cell inside the parallel-connected cells. The input variables are the total current and total voltage of the parallel-connected cells, while the output is the SOC of each cell. The specific derivation procedure of the Kalman Filtering algorithm is presented in Equations (50) ~ (75). In this method, the established ECM of parallel-connected cells is discretized and the Kalman Filtering algorithm is linearized. Few researches have been found on state of charge estimation of parallel-connected battery pack [36].

The first step is discretization of the state space matrix of each single cell. The model of each cell after discretization is shown in Equations (50) ~ (62).

$$V_{oc,k+1} = V_{oc,k} + \frac{i_{cell,k}}{M_k}\Delta t + w_{1,k} \qquad (50)$$

$$M_k = 3600 Q_{cell} \frac{dSOC}{dV_{oc}}|_k \qquad (51)$$

$$V_{P1,k+1} = V_{P1,k}\exp(-\Delta t / \tau_{p1,k}) + R_{P1,k} i_{cell,k}(1-\exp(-\Delta t / \tau_{P1,k})) + w_{2,k} \qquad (52)$$

$$V_{P2,k+1} = V_{P2,k}\exp(-\Delta t / \tau_{P2,k}) + R_{P2,k} i_{cell,k}(1-\exp(-\Delta t / \tau_{P2,k})) + w_{3,k} \qquad (53)$$

$$V_{t,k} = V_{oc,k} + V_{P1,k} + V_{P2,k} + R_{D,k} i_{cell,k} \qquad (54)$$

Thus, it can be deduced:

$$\begin{bmatrix} V_{oc,k+1} \\ V_{P1,k+1} \\ V_{P2,k+1} \end{bmatrix} = \begin{bmatrix} 1 & 0 & 0 \\ 0 & e^{-\Delta t/\tau_{P1,k}} & 0 \\ 0 & 0 & e^{-\Delta t/\tau_{P2,k}} \end{bmatrix} \begin{bmatrix} V_{oc,k} \\ V_{P1,k} \\ V_{P2,k} \end{bmatrix} + \begin{bmatrix} \frac{\Delta t}{M_k} \\ R_{P1,k}(1-e^{-\Delta t/\tau_{P1,k}}) \\ R_{P2,k}(1-e^{-\Delta t/\tau_{P2,k}}) \end{bmatrix} \begin{bmatrix} i_{cell,k} \end{bmatrix} + w_k \qquad (55)$$

$$\begin{bmatrix} V_{t,k} \end{bmatrix} = \begin{bmatrix} 1 & 1 & 1 \end{bmatrix} \begin{bmatrix} V_{oc,k} \\ V_{P1,k} \\ V_{P2,k} \end{bmatrix} + \begin{bmatrix} R_{D,k} \end{bmatrix} \begin{bmatrix} i_{cell,k} \end{bmatrix} + v_k \qquad (56)$$

$$x_k = \begin{bmatrix} V_{oc,k} \\ V_{P1,k} \\ V_{P2,k} \end{bmatrix} \quad (57)$$

$$u_k = \begin{bmatrix} i_{cell,k} \end{bmatrix} \quad (58)$$

$$A_k = \begin{bmatrix} 1 & 0 & 0 \\ 0 & e^{-\Delta t/\tau_{P1,k}} & 0 \\ 0 & 0 & e^{-\Delta t/\tau_{P2,k}} \end{bmatrix} \quad (59)$$

$$B_k = \begin{bmatrix} \dfrac{\Delta t}{M_k} \\ R_{P1,k}(1-e^{-\Delta t/\tau_{P1,k}}) \\ R_{P2,k}(1-e^{-\Delta t/\tau_{P2,k}}) \end{bmatrix} \quad (60)$$

$$C_k = [1 \quad 1 \quad 1] \quad (61)$$

$$D_k = \begin{bmatrix} R_{D,k} \end{bmatrix} \quad (62)$$

The second step is the construction of parallel-connected cells through the state space matrix of each single cell, as shown in Equations (63) ~ (70).

$$\begin{cases} X_{k+1} = A'_k X_k + B'_k U_k + w_k \\ Y_k = C'_k X_k + D'_k U_k + v_k \end{cases} \quad (63)$$

$$Y_k = V_{t,k}, U = i_k \quad (64)$$

$$X_k = \begin{bmatrix} V_{oc,1,k}; & V_{P1,1,k}; & V_{P2,1,k}; & V_{oc,2,k}; & V_{P1,2,k}; & V_{P2,2,k}; & V_{oc,3,k}; & V_{P1,3,k}; & V_{P2,3,k}; \end{bmatrix} \quad (65)$$

Among which,

$$\begin{aligned} A'_k &= A_k + B_k H_k G_k^{-1} E_k \\ B'_k &= B_k H_k G_k^{-1} F_k \\ C'_k &= C_k + D_k H_k G_k^{-1} E_k \\ D'_k &= D_k H_k G_k^{-1} F_k \end{aligned} \quad (66)$$

$$E_k = \begin{bmatrix} 0 & 0 & 0 & 0 & 0 & 0 & 0 & 0 & 0 \\ -1 & -1 & -1 & 1 & 1 & 1 & 0 & 0 & 0 \\ 0 & 0 & 0 & -1 & -1 & -1 & 1 & 1 & 1 \end{bmatrix} \quad (67)$$

$$F_k = \begin{bmatrix} 1 \\ 0 \\ 0 \end{bmatrix} \quad (68)$$

$$G_k = \begin{bmatrix} 1 & 0 & 0 \\ R_{D,1,k} + R_{f,1} & -(R_{D,1,k} + +R_{f,1} + R_{D,2,k} + R_{f,2} + R_{c,2}) & R_{D,2,k} + R_{f,2} \\ 0 & R_{D,2,k} + R_{f,2} & -(R_{D,2,k} + R_{f,2} + R_{D,3,k} + R_{f,3} + R_{c,3}) \end{bmatrix}$$

(69)

$$H_k = \begin{bmatrix} 1 & -1 & 0 \\ 0 & 1 & -1 \\ 0 & 0 & 1 \end{bmatrix} \quad (70)$$

The third step is the Kalman Filtering process after discretization according to Kalman Filtering theory, as shown in Equations (71) ~ (75).

State estimate time update:

$$\hat{X}_{k|k-1} = A'_{k-1}\hat{X}_{k-1|k-1} + B'_{k-1}U'_{k-1} \quad (71)$$

Error covariance time update:

$$P_{k|k-1} = A'_{k-1}P_{k-1|k-1}A'^{T}_{k-1} + \Sigma_w \quad (72)$$

Kalman gain calculation:

$$L_k = P_{k|k-1}C'^{T}_k[C'_k P_{k|k-1}C'^{T}_k + \Sigma_v]^{-1} \quad (73)$$

State estimate measurement update:

$$\hat{X}_{k|k} = \hat{X}_{k|k-1} + L_k[Y_k - C'_k\hat{X}_{k|k-1} - D'_k U_k] \quad (74)$$

Error covariance measurement update:

$$P_{k|k} = (I - L_k C'_k)P_{k|k-1} \quad (75)$$

The SOC estimation results of the steady 1/3C discharge process are shown in Figure 13. The solid line represents the experimental results, while the dashed line represents the simulation results.

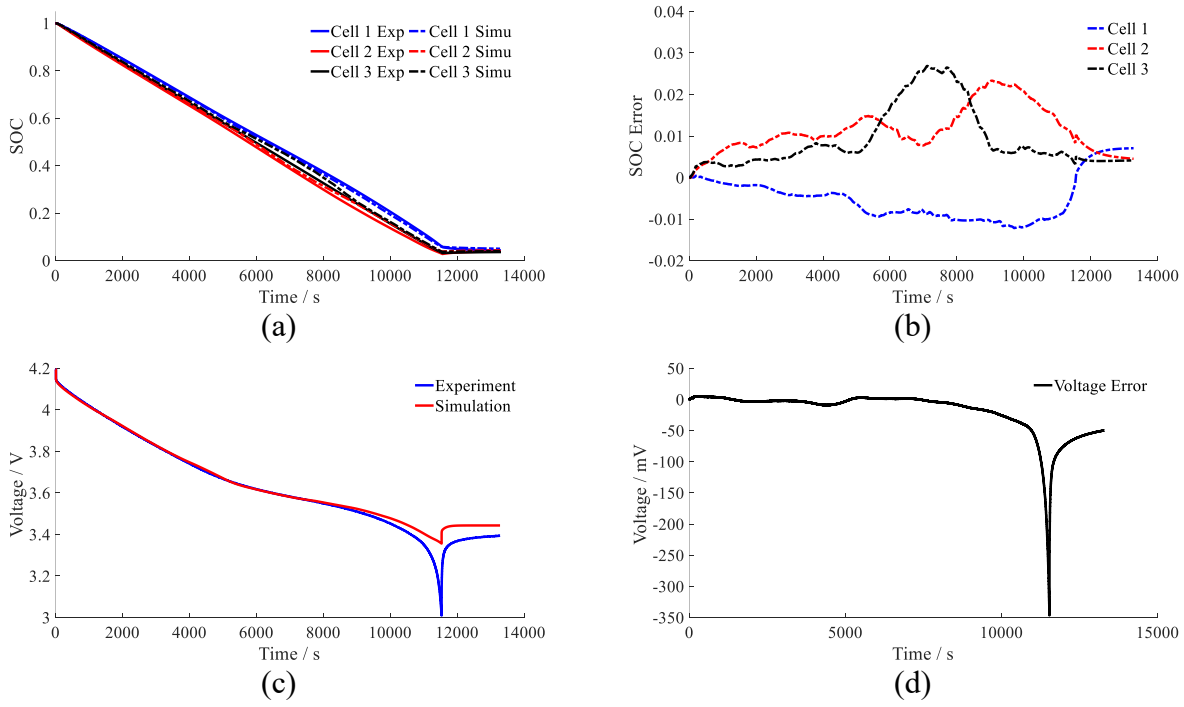

Figure 13. SOC estimation of ECM for batteries connected in parallel, solid line = experiment, dashed line = simulation, (a) SOC for each cell, (b) SOC estimation error for each cell, (c) terminal voltage for experiment and model, (d) terminal voltage error

The SOC estimation is described in Figure 13(a), and the SOC error in Figure 13(b). The SOC estimation error was less than 3% under all operating conditions. The battery module voltage and error are shown in Figure 13(c) ~ (d). We can see that, the voltage error was less than 25 mV from 20% to 100% SOC, while the voltage error increased rapidly in the low SOC region because of the low model accuracy.

The SOC estimation results of the steady 1/3C charge process are shown in Figure 14. The SOC estimation results and error are described in Figure 14(a) ~ (b). The SOC estimation error was less than 4% under all operating conditions, which was slightly worse than the results above. The battery module voltage and error are shown in Figure 14(c) ~ (d). The voltage error was less than 25 mV in most SOC regions. However, a steady-state voltage error appeared when the batteries were fully charged, which should be reduced.

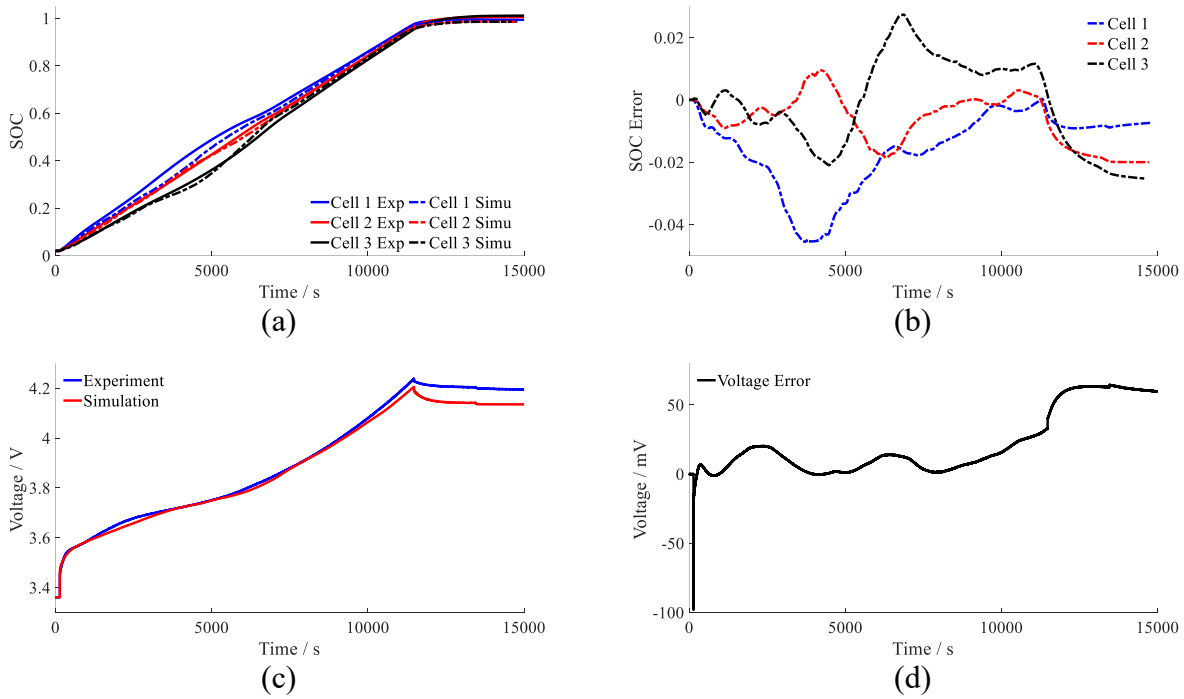

Figure 14. SOC estimation of ECM for batteries connected in parallel, solid line = experiment, dashed line = simulation, (a) SOC for each cell, (b) SOC estimation error for each cell, (c) terminal voltage for experiment and model, (d) terminal voltage error

5. CONCLUSIONS

An equivalent circuit model (ECM) of a battery pack composing N cells connected in parallel is introduced in this paper. The parameters in the ECM of single cells are identified by optimization algorithms. In addition, the battery open circuit voltage V_{oc} and polarization voltage drop V_P are chosen as state variables by applying state space theory and Kirchhoff's current and voltage laws to establish the ECM of cell packs. The results conclude that the model accuracy of the ECM of cells connected in

parallel is relatively high not only in the steady charge/discharge process but also in the dynamic stress tests.

Furthermore, a Kalman Filtering algorithm based on the aforementioned ECM is proposed for the SOC estimation of battery packs connected in parallel. The total current and the total voltage of parallel-connected battery packs are used as input variables of the ECM, which is linearized by the Kalman Filtering method, and the equivalent circuit model of a single cell is discretized. The results conclude that the proposed SOC estimation method for cells connected in parallel has good prediction accuracy.

Furthermore, the ECM proposed in this paper can be applied for the follow-up battery module design in the parallel configuration and integral SOC estimation of the individual cells connected in parallel.

ACKNOWLEDGMENTS
This work is supported by the Ministry of Science and Technology of China (Grant No. 2018YFB0104404 and No. 2016YFE0102200); the China Postdoctoral Science Foundation (Grant No. 2017M610086); and the National Natural Science Foundation of China (Grant No. 51706117 and Grant No. U1564205).

References

1. X. Chen, W. Lu, C. Chen, M. Xue, *Int. J. Elecrtrochem. Sci*., 13 (2018) 296.
2. X. Jiang, Z. Yuan, J. Liu, X. Jin, L. Jin, P. Dong, Y. Zhang, Y. Yao, Q. Cheng, C. Liu, Y. Zhang, X. Yu, *Int. J. Electrochem. Sci*., 13 (2018) 2341.
3. X. Feng, J. Li, L. Lu, J. Hua, L. Xu, M. Ouyang, *J. Power Sources*, 209 (2012) 30.
4. Y. Wang, C. Zhang, Z. Chen, *J. Power Sources*, 279 (2015) 306-311..
5. Y. Wang, C. Zhang, Z. Chen, *Appl. Energ.*, 135 (2014), 81-87.
6. X. Lai, Y. Zheng, T. Sun, *Electrochimica Acta*, 259 (2018) 566-577.
7. X. Feng, J. Li, M. Ouyang, L. Lu, J. Li, X. He, *J. Power Sources*, 232 (2013) 209.
8. C. Weng, X. Feng, J. Sun, H. Peng, *Appl. Energ.*, 180 (2016) 360.
9. W. Song, M. Chen, F. Bai, S. Lin, Y. Chen, Z. Feng, *Appl. Therm. Eng.*, 128 (2018) 1165.
10. Y. Zhu, F. Yan, J. Kang, C. Du, *Int. J. Electrochem. Sci.*, 12 (2017) 6895.
11. S. Wang, L. Shang, Z. Li, H. Deng, Y. Ma, *Int. J. Electrochem. Sci.*, 10 (2015) 5130.
12. Y. Zhu, F. Yan, J. Kang, C. Du, *Int. J. Electrochem. Sci.*, 12 (2017) 6895.
13. Y. Zhu, F. Yan, J. Kang, C. Du, *Int. J. Electrochem. Sci.*, 12 (2017) 6895.
14. M. Hu, J. Wang, C. Fu, D. Qin, S. Xie, *Int. J. Electrochem. Sci.*, 11 (2016) 577.
15. G. Zhao, F. Xu, *Int. J. Electrochem. Sci.*, 13 (2018) 8543.
16. J. Zhao, Y. Gao, J. Guo, L. Chu, A.F. Burke, *Int. J. Electrochem. Sci.*, 13 (2018) 1773.
17. X. Feng, X. He, L. Lu, M. Ouyang, *J. Electrochem. Soc.*, 165(2) (2018) A155.
18. C. Pastor-Fernándeza, T. Bruena,W. D. Widanagea, M. A. Gama-ValdezbJ.Marcoa, *J. Power Sources*, 329 (2016) 574-585.
19. R. Gogoana, M. B. Pinson, M. Z. Bazant, S. E. Sarma, *J. Power Sources*, 252 (2014) 8-13.
20. N. Yang, X. Zhang, B. Shang, G. Li, *J. Power Sources*, 306 (2016) 733-741.
21. R. Spurrett, C. Thwaite, A. Holland, D. Lizius, G.J. Dudley, *J. Space Power*, Conf. (2002) 685e691.
22. D. Fouchard, J.B. Taylor, *J. Power Sources*, 21 (1987) 195e205.
23. B.A. Cole, R.J. Schmitt, J. Szymborski, *20th Int. Telecommun. Energy Conf. (INTELEC)* (1998)

356e363.
24. J. Zhang, S. Ci, H. Sharif, M. Alahmad, *IEEE Trans. Energy Convers.* 25 (2010) 1133e1141.
25. M. Wu, C. Lin, Y. Wang, C. Wan, C. R. Yang, *J. Electrochimica Acta*, 52(3), (2006) 1349-1357.
26. W. Shi, X. Hu, C. Jin, J. Jiang, Y. Zhang, T. Yip, *J. Power Sources*, 313 (2016) 198-204.
27. C. Weng, X. Feng, J. Sun, H. Peng, *Appl. Energ.*, 180 (2016) 360-368.
28. F. An, J. Huang, C. Wang, Z. Li, J. Zhang, S. Wang, P. Li, *J. Energ. Stor.*, 6 (2016) 195-203.
29. M. Dubarry, A. Devie, B. Y. Liaw, *J. Power Sources*, 321 (2016) 36-46.
30. G. J. Offer, V. Yufit, D. A. Howey, B. Wu, N. P. Brandon, *J. Power Sources*, 206 (2012) 383-392.
31. S. Miyatake, Y. Susuki, T. Hikihara, S. Itoh, K. Tanaka, *J. Power Sources*, 241 (2013) 736-743
32. Y. Wang, X. Zhang, C. Liu, R. Pan, Z. Chen, *J. Power Sources*, 389(2018), 93-105.
33. T. Bruen, J. Marco, *J. Power Sources*, 310(2016), 91-101.
34. M. J. Brand, M. H. Hoffman, M. Steinhardt, S. F. Schuster, A. Jossen, *J. Power Sources*, 334(2016), 202-212.
35. G. L. Plett, *J. Power Sources*, 134(2004), 252-261.
36. F. Sun, R. Xiong, *J. Power Sources*, 274(2015), 582-594.